NANO · MICRO small
www.small-journal.com

A Crystalline-Water Electrolyte Enabled High Depth-of-Discharge Anodes in Aqueous Zinc Metal Batteries

*Rui Yao, Yunxiang Zhao, Lumeng Wang, Feiyu Kang, Johnny C. Ho, Chunyi Zhi, and Cheng Yang**

Aqueous zinc metal batteries are regarded as a promising energy storage solution for a green and sustainable society in the future. However, the practical application of metallic zinc anode is plagued by the thermodynamic instability issue of water molecules in conventional electrolytes, which leads to severe dendrite growth and side reactions. In this work, an ultra-thin and high areal capacity metallic zinc anode is achieved by utilizing crystalline water with a stable stoichiometric ratio. Unlike conventional electrolytes, the designed electrolyte can effectively suppress the reactivity of water molecules and diminish the detrimental corrosion on the metallic zinc anode, while preserving the inherent advantages of water molecules, including great kinetic performance in electrolytes and H^+ capacity contribution in cathodes. Based on the comprehensive performance of the designed electrolyte, the 10 µm Zn||10 µm Zn symmetric cell stably ran for 1000 h at the current density of 1 mA cm^{-2}, and the areal capacity of 1 mAh cm^{-2}, whose depth-of-discharge is over 17.1%. The electrochemical performance of the 10 µm Zn||9.3 mg cm^{-2} polyaniline (PANI) full-cell demonstrates the feasibility of the designed electrolyte. This work provides a crucial understanding of balancing activity of water molecules in aqueous zinc metal batteries.

1. Introduction

Aqueous zinc metal batteries have been rising as one of the most promising candidates for advanced energy storage owing to a series of advantages such as high capacity, low cost, and environmental benignity.[1] However, due to the thermodynamic instability issue of conventional aqueous electrolytes, parasitic reactions such as dendrite growth, by-product formation, and hydrogen evolution often inevitably take place during zinc plating/stripping, which poses great challenges for realizing high-performance metallic zinc anodes.[2]

To date, intensive explorations have been made in developing novel electrolytes. Among them, rationally regulating the zinc salt concentration has been recognized as one of the most effective methods. The broadly studied highly concentrated electrolyte system can inhibit dendrite growth by preventing zinc salt depletion;[3] ultra-low concentration electrolytes can suppress by-product formation and widen the electrochemical stable window by dramatically decreasing the amount of active hydrated ions.[4] Introducing functional additives is another feasible option. Ionic surfactants, such as multivalent metal salts and quaternary ammonium salts can regulate the electrochemical process of zinc plating/stripping via electrostatic interaction.[5] Small molecular additives like glucose and glycine can regulate the parasitic reactions and promote the formation of solid electrolyte interphase via selective surface adsorption.[6] Organic co-solvents, such as N-methyl-pyrrolidone (NMP) and dimethyl methylphosphonate (DMMP) can regulate zinc solvation structures and the activity of water molecules via hydrogen bond interactions.[7] The above cases highlighted the critical role of electrolyte engineering in enhancing the electrochemical performance of aqueous zinc metal batteries.

In practical applications, maximizing the utilization rate of the electrodes is indispensable for elevating the battery performance. For example, the negative and positive (N/P) capacity ratio of commercial lithium-ion batteries is usually ≈1.1, whose negative electrode capacity is only slightly higher than the positive electrode capacity. However, excessive anode loading of metallic zinc has been widely adopted in the currently reported electrochemical testing protocols. This is simply because the surplus loading can offset the negative effects of parasitic reactions during zinc plating/stripping, which significantly consume the active metallic zinc.[8] Such a situation is more pronounced in aqueous electrolytes. As the standard electrode potential of zinc (−0.76 V vs SHE) is lower than that of hydrogen (0 V vs SHE), the presence of water can easily trigger severe side reactions (i.e., hydrogen evolution and by-product formation). Employing aprotic electrolytes can avoid water-induced side reactions, yet the capacity of most reported cathodes declines substantially without H^+,

R. Yao, Y. Zhao, L. Wang, F. Kang, C. Yang
Institute of Materials Research
Tsinghua Shenzhen International Graduate School
Tsinghua University
Shenzhen 518055, China
E-mail: yang.cheng@sz.tsinghua.edu.cn
J. C. Ho, C. Zhi
Department of Materials Science and Engineering
City University of Hong Kong
Kowloon, Hong Kong 999077, China

The ORCID identification number(s) for the author(s) of this article can be found under https://doi.org/10.1002/smll.202404865

DOI: 10.1002/smll.202404865

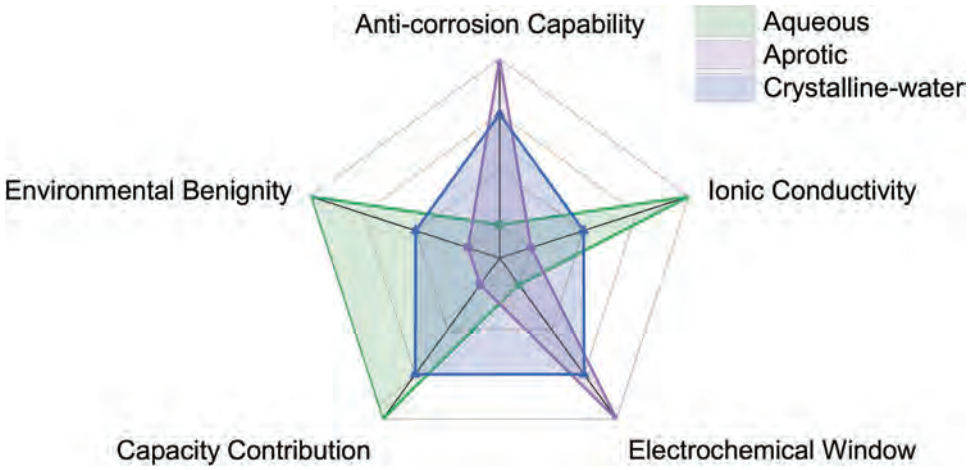

Figure 1. A radar plot analysis of different electrolytes. The aqueous electrolyte refers to the system that zinc salts are dissolved in the solvent water. The aprotic electrolyte refers to the system that anhydrous zinc salts are dissolved in aprotic solvents. The crystalline-water electrolyte refers to the designed electrolyte in this work that hydrated zinc salts dissolved in aprotic solvents, which exhibits more comprehensive performances.

and the kinetic performance of the cell also gets worse.[9] How to effectively regulate the activity of water molecules while preserving the inherent advantages of water molecules is a critical challenge that limits the further development of aqueous zinc metal batteries.[10]

In this work, we achieved an ultra-thin and high areal capacity metallic zinc anode by utilizing the crystalline water with a stoichiometric ratio. As shown in **Figure 1**, different from conventional electrolytes, the designed electrolyte can effectively suppress the reactivity of water molecules and diminish the detrimental corrosion on the metallic zinc anode, while preserving the inherent advantages of water molecules, including great kinetic performance in electrolytes and the H^+ capacity contribution in cathodes. Based on the comprehensive performance of the designed electrolyte, the 10 µm Zn||10 µm Zn symmetric cell stably ran 1000 h at the current density of 1 mA cm^{-2} and the areal capacity of 1 mAh cm^{-2}. The 10 µm Zn||10 µm Zn symmetric cell stably ran for 750 h at the current density of 2 mA cm^{-2} and the areal capacity of 1 mAh cm^{-2}. The 10 µm Zn||20 µm Ti half-cell exhibited the average Coulombic efficiency of 99.3% within 75 cycles. 10 µm Zn||9.3 mg cm^{-2} PANI full-cells stably ran 129 cycles with a capacity retention of 87.6%, which demonstrated the feasibility of the designed electrolyte in energy storage devices.

2. Results and Discussion

As a representative organic reagent featuring low viscosity, low toxicity, low water solubility, excellent chemical stability, and low density, dimethyl carbonate (Figure S1, Supporting Information DMC) was adopted as the aprotic solvent. Above all, to ensure the purity and consistency of the electrolytes, we evaluated the solubility of different hydrated zinc salts in DMC solvent (Figure S2, Supporting Information). 1 M $Zn(ClO_4)_2{\cdot}6H_2O$ was completely dissolved in DMC solvent, but there was evident undissolved precipitate in both 1 M $ZnSO_4{\cdot}7H_2O$ and 1 M $Zn(CH_3COO)_2{\cdot}2H_2O$. Therefore, we adopted the zinc perchlorate hexahydrate as zinc salt to ensure excellent ionic transport. Furthermore, we conducted the solubility test of zinc salts with/without crystalline water (Figure S3, Supporting Information). 1 M $Zn(ClO_4)_2{\cdot}6H_2O$ was completely dissolved in water (H_2O) solvent like in DMC solvent. However, as a representative of anhydrous zinc salts, 1 M $Zn(OTF)_2$ was unable to completely be dissolved in DMC solvent even after ultrasonic treatment. After reducing the concentration of anhydrous zinc salts, although the turbidity of the solution was decreased, 0.5 M $Zn(OTF)_2$ could not still be dissolved in DMC solvent. Therefore, we adopted the zinc perchlorate hexahydrate dissolved in H_2O solvent as the control electrolyte and the zinc perchlorate hexahydrate dissolved in DMC solvent as the designed electrolyte. The control electrolyte was prepared by dissolving 1 M $Zn(ClO_4)_2{\cdot}6H_2O$ into the deionized water, which was marked as E(H_2O). The designed electrolyte was prepared by dissolving 1 M $Zn(ClO_4)_2{\cdot}6H_2O$ into the dimethyl carbonate, which was marked as E(DMC). Above all, we evaluated the physicochemical properties of both electrolytes. As shown in **Figure 2a**, the ionic conductivity of E(DMC) was 7.7 mS cm^{-1}, which was lower than that of E(H_2O). But benefiting from the low viscosity of dimethyl carbonate solvent, the viscosity of E(DMC) was 3.3 mPa s, which did not significantly increase compared with the E(H_2O). To evaluate the impact of introducing $Zn(ClO_4)_2{\cdot}6H_2O$ on the original solvent environments, we first conducted attenuated total reflectance (ATR) infrared spectroscopy on both pure solvents and electrolytes. As shown in Figure 2b, the —OH stretching vibration peak ≈3300 cm^{-1} blueshifted and the bending vibration peak of water molecules ≈1630 cm^{-1} redshifted after introducing $Zn(ClO_4)_2{\cdot}6H_2O$. The —CH_3 stretching vibration ≈2960 cm^{-1} blueshifted and the —C═O stretching vibration of dimethyl carbonate molecules ≈1750 cm^{-1} redshifted after introducing $Zn(ClO_4)_2{\cdot}6H_2O$. It suggests that there are similar hydrogen bond interactions between $Zn(ClO_4)_2{\cdot}6H_2O$ with both water molecules in E(H_2O) and dimethyl carbonate molecules in E(DMC). Besides, the —OH stretching vibration peak and the bending vibration peak of water molecules were also observed in E(DMC), whose wavenumbers were evidently higher than that in E(H_2O).[11] It indicates that the hydrogen bond interaction in E(DMC) is significantly stronger than that in E(H_2O). As shown in Figure 2c, we also observed the weak —OH stretching vibration

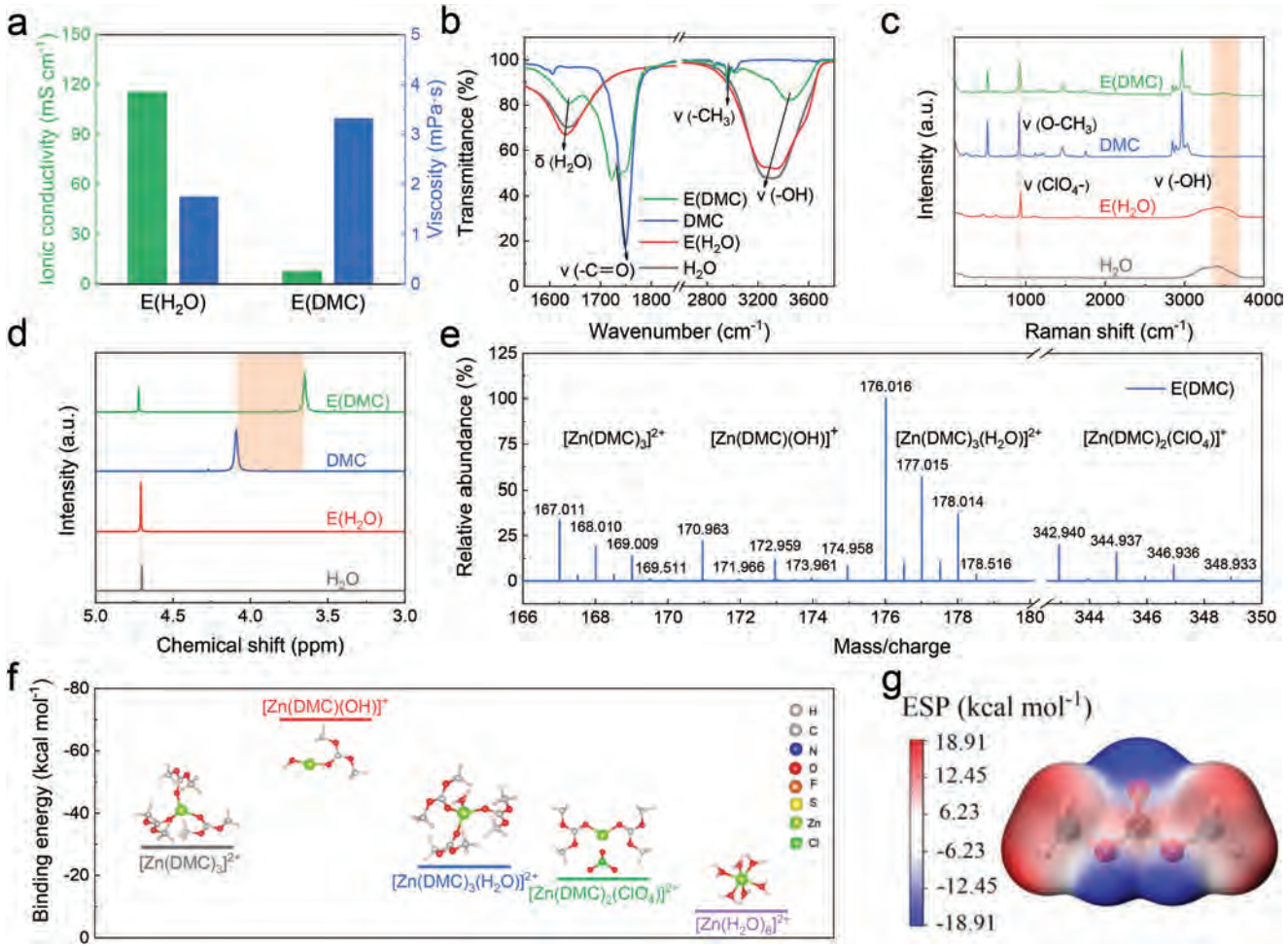

Figure 2. Characterizations of the electrolytes. a) Ionic conductivity and viscosity of both electrolytes. b) Attenuated total reflectance infrared spectroscopy of both electrolytes and solvents. c) Raman spectroscopy of both electrolytes and solvents. d) Nuclear magnetic resonance of both electrolytes and solvents. e) High-resolution mass spectroscopy of E(DMC). f) Binding energy of different solvation structures. g) Electrostatic potential distribution map of dimethyl carbonate molecules.

peak of water molecules ≈3500 cm^{-1} and the coupling signal of ClO_4^- stretching vibration ≈930 cm^{-1} and O—CH_3 stretching vibration ≈915 cm^{-1} in Raman spectroscopy.[12] To verify the hydrogen bond interaction differences, we performed nuclear magnetic resonance (NMR) ^{1}H spectroscopy on both pure solvents and electrolytes. As shown in Figure 2d, the chemical shift of the characteristic signal of water molecules slightly increased after introducing $Zn(ClO_4)_2{\cdot}6H_2O$. It confirms that the macroscopic hydrogen bond interaction in E(H_2O) is negligible since the water content is dominant. However, the relative chemical shift of the characteristic signal of dimethyl carbonate significantly decreased after introducing $Zn(ClO_4)_2{\cdot}6H_2O$. It indicates that the macroscopic hydrogen bond interaction in E(DMC) is significant since the water content is limited. To further clarify the specific impact on the solvation environments, we conducted high-resolution mass spectroscopy (HRMS). As shown in Figure 2e, several solvation structures such as $[Zn(DMC)_3]^{2+}$, $[Zn(DMC)(OH)]^+$, $[Zn(DMC)_3(H2O)]^{2+}$, and $[Zn(DMC)(ClO_4)]^+$ could be observed in E(DMC). Different from the solvation structures dominated by water molecules in E(H_2O), the newly-formed solvation structures involved a large number of dimethyl carbonate molecules and anions. According to the relative abundance, the major content of the solvation structure could be contributed by $[Zn(DMC)_3(H_2O)]^{2+}$. The above results confirm that the solvation environment in E(DMC) undergoes significant changes after the dominant position of water content is converted. To further verify the solvation structure changes in E(DMC), we conducted theoretical computation based on the density functional theory. As shown in Figure 2f, the binding energies of $[Zn(DMC)_3]^{2+}$, $[Zn(DMC)(OH)]^+$, $[Zn(DMC)_3(H_2O)]^{2+}$, and $[Zn(DMC)_2(ClO_4)]^+$ were −29.01, −69.98, −22.76, and −18.85 kcal mol^{-1}, respectively. However, the binding energy of $[Zn(H_2O)_6]^{2+}$ was −8.53 kcal mol^{-1}, which was more positive than the newly formed solvation structures in E(DMC). It confirms that zinc ions tend to coordinate with dimethyl carbonate molecules and anions rather than water molecules in E(DMC). To further explore the differences in solvation structures, we simulated the electrostatic potential distribution of both solvent molecules. The electrostatic potential of hydrogen atoms in the water molecules was relatively positive, so they mainly

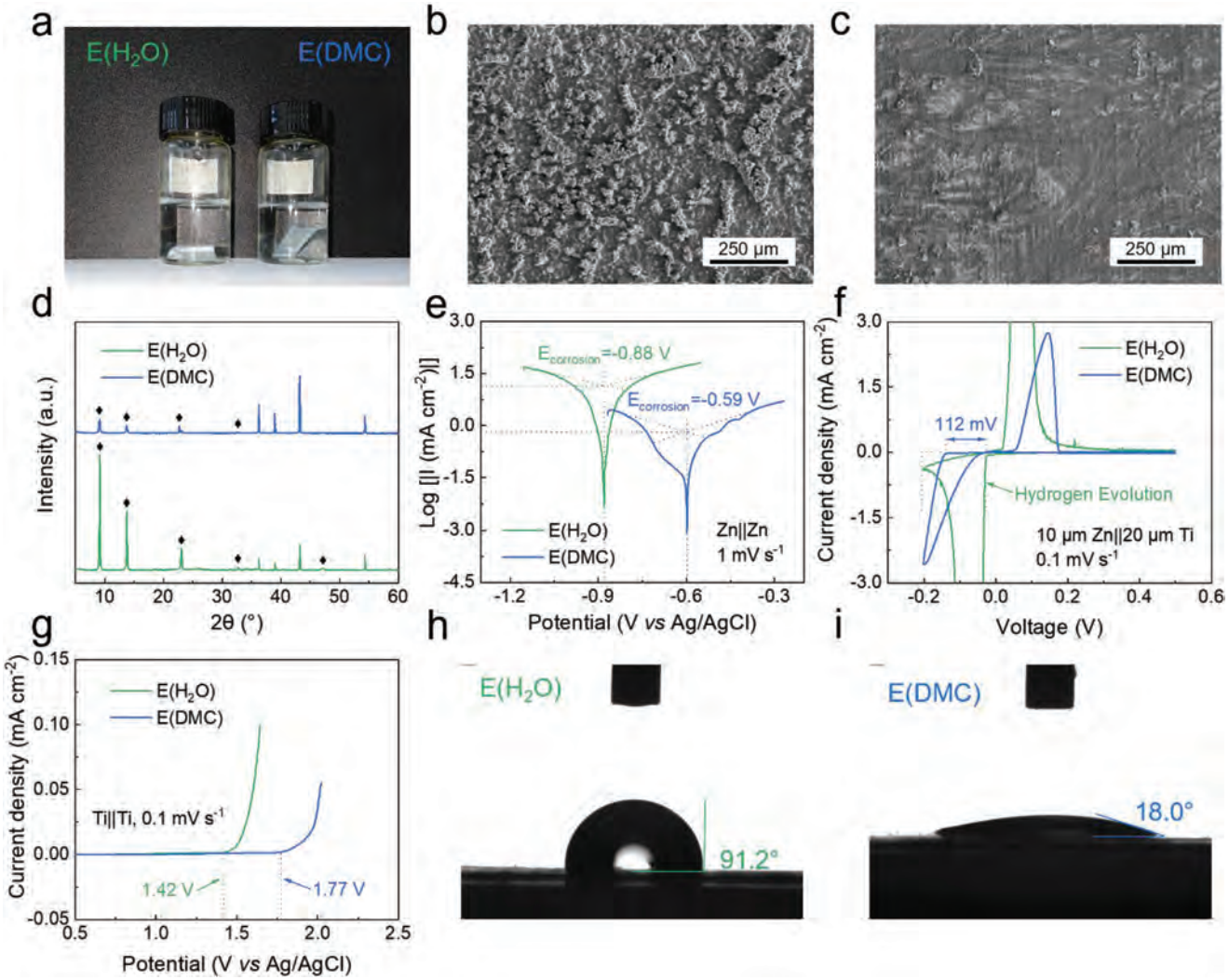

Figure 3. Characterizations of the electrodes. a) Photographic image of the zinc foil soaking test in both electrolytes. b) SEM image of the metallic zinc after the two-week soaking test in E(H2O). c) SEM image of the metallic zinc after the two-week soaking test in E(DMC). d) X-ray diffraction patterns of the metallic zinc after the two-week soaking test in both electrolytes. e) Linear polarization curves of Zn||Zn symmetric cells with both electrolytes. f) Cyclic voltammetry curves of Zn||Ti half-cell with both electrolytes. g) Linear scanning voltammetry tests of both electrolytes. h) Contact angle test of E(H2O) on the metallic zinc. i) Contact angle test of E(DMC) on the metallic zinc.

coordinated with zinc ions through oxygen atoms with more negative potential (Figure S4, Supporting Information). Similarly, as shown in Figure 2g, the potential of $-CH_3$ in dimethyl carbonate molecules was relatively positive, so they tended to coordinate with zinc ions through oxygen atoms with more negative potential. The above results demonstrated the solvation environment difference of both electrolytes.

Furthermore, we performed a soaking test to investigate the chemical stability of the metallic zinc anode in both electrolytes. As shown in **Figure** 3a, the ultra-thin metallic zinc was soaked in both electrolytes for two weeks. As shown in Figure 3b,c, the scanning electron microscopy (SEM) image of the metallic zinc soaked in E(H_2O) for two weeks showed that massive corrosion products were distributed on the surface of the metallic zinc. Differently, very few corrosion by-products were observed on the surface of the metallic zinc soaked in E(DMC) (Figure S5, Supporting Information). Energy dispersive spectroscopy mapping showed that the signal intensity of Zn atoms was weaker but the signal intensity of Cl atoms was comparatively stronger on the metallic zinc soaked in E(H_2O) (Figure S6, Supporting Information). However, the signal intensity of Zn was stronger than that of Cl atoms on the metallic zinc soaked in E(DMC) (Figure S7, Supporting Information). This suggests that more corrosion by-products were formed on the metallic zinc being soaked in E(H_2O) than in E(DMC). To further verify the above results, we employed X-ray diffraction spectroscopy. As shown in Figure 3d, a significant signal intensity of the corrosion by-products was observed on the surface of the metallic zinc being soaked in E(H_2O). However, the stronger signal intensity of the metallic zinc rather than the corrosion by-products was observed on the metallic zinc being soaked in E(DMC). Besides, we

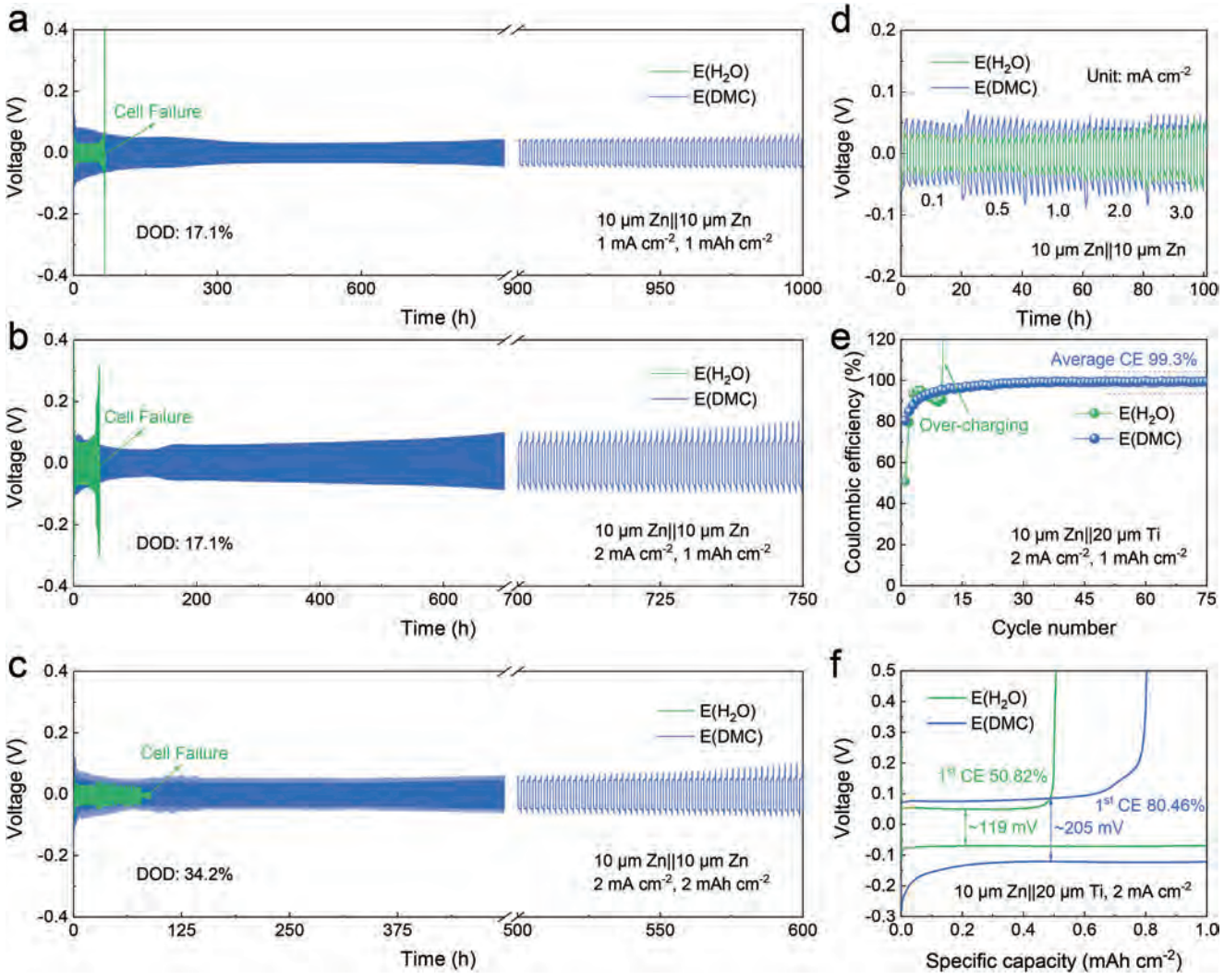

Figure 4. Galvanostatic cycling of the electrodes. a) Galvanostatic cycling of the Zn||Zn symmetric cells with both electrolytes at the current density of 1 mA cm^{-2} and the areal capacity of 1 mAh cm^{-2}. b) Galvanostatic cycling of the Zn||Zn symmetric cells with both electrolytes at the current density of 2 mA cm^{-2} and the areal capacity of 1 mAh cm^{-2}. c) Galvanostatic cycling testing result of the Zn||Zn symmetric cells with both electrolytes at the current density of 2 mA cm^{-2} and the areal capacity of 2 mAh cm^{-2}. d) Rate capability test of the Zn||Zn symmetric cells with both electrolytes. e) Coulombic efficiency tests of the Zn||Ti half-cells with both electrolytes at the current density of 2 mA cm^{-2} and the areal capacity of 1 mAh cm^{-2}. f) Charge and discharge curves of the Zn||Ti half-cells with both electrolytes at the current density of 2 mA cm^{-2} and the areal capacity of 1 mAh cm^{-2}.

collected the linear polarization curves to further verify the chemical stability of the metallic zinc in both electrolytes from the perspective of electrochemical methods. As shown in Figure 3e, the corrosion potential of the metallic zinc was ≈−0.88 V (vs Ag/AgCl) in E(H_2O), but the corrosion potential of the metallic zinc was ≈−0.59 V (vs Ag/AgCl) in E(DMC). Meanwhile, the fitted corrosion current density of the metallic zinc in E(H_2O) was higher than that in E(DMC). It confirms that metallic zinc is thermodynamically and kinetically easier to be corroded in E(H_2O) compared to that in E(DMC). To investigate the difference of metallic zinc during cycling in both electrolytes, we conducted the cyclic voltammetry test at the scan rate of 0.1 mV s^{-1}. Similar electrochemical redox peaks were observed in the Zn||Ti half-cells with both electrolytes (Figure S8, Supporting Information). Differently, as shown in Figure 3f, although the Zn||Ti half-cell with E(H_2O) exhibited a higher current density response, there were evident fluctuations during zinc deposition. This suggests that a competitive hydrogen evolution reaction takes place in E(H_2O) during zinc deposition. However, the metallic zinc exhibits a stable and reversible plating/stripping behavior in E(DMC). To fully evaluate the electrochemical stability, we conducted the linear scanning voltammetry test for both electrolytes. As shown in Figure 3g, E(H_2O) started to oxidize at 1.42 V (vs Ag/AgCl), but E(DMC) started to oxidize until 1.77 V (vs Ag/AgCl). This indicates that the electrochemical oxidation stability of E(DMC) is evidently better than that of E(H_2O). Besides, to evaluate the wettability of both electrolytes on the metallic zinc, we conducted the contact angle tests. As shown in Figure 3h,i, the contact angle of E(H_2O) on the metallic zinc was 91.2°, which was notably higher than 18.0° of E(DMC) on the metallic zinc. It suggests that the wettability of E(DMC) on the metallic zinc is better than that of E(H_2O). As demonstrated in the above results, the unique

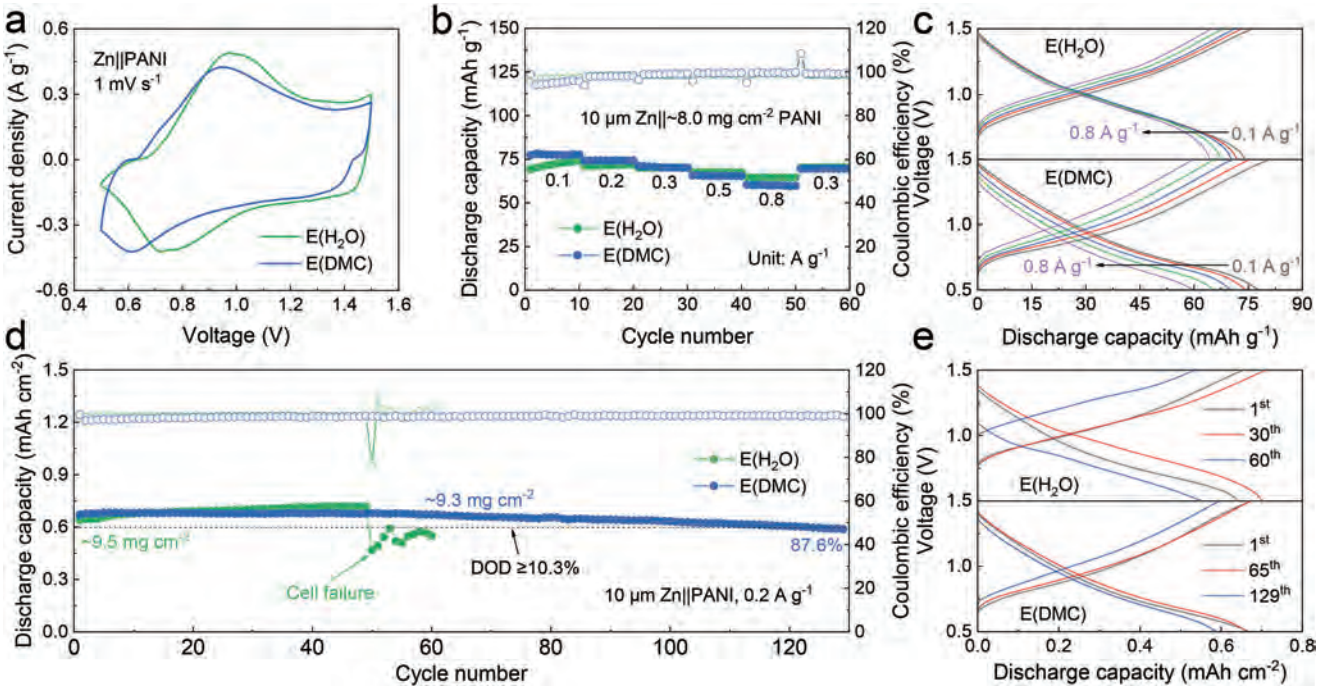

Figure 5. Electrochemical performance of Zn||PANI full cells. a) Cyclic voltammetry curves of Zn||PANI full-cells with both electrolytes at the scan rate of 1 mV s^{-1}. b) Rate capability test of Zn||PANI full-cells with both electrolytes at different current densities. c) Charge and discharge curves of Zn||PANI full-cells with both electrolytes at different current densities. d) Galvanostatic cycling of Zn||PANI full-cells with both electrolytes at the current density of 0.2 A g^{-1}. e) Charge and discharge curves of Zn||PANI full-cells with both electrolytes at the current density of 0.2 A g^{-1}.

solvation environment of E(DMC) confers superior affinity and stability for metallic zinc.

To further evaluate the zinc plating/stripping difference of the metallic zinc in both electrolytes, we conducted the galvanostatic cycling tests. As shown in **Figure** 4a, the 10 μm Zn||10 μm Zn symmetric cells with E(H_2O) failed after 66 h at the current density of 1 mA cm^{-2} and the areal capacity of 1 mAh cm^{-2}. The 10 μm Zn||10 μm Zn symmetric cells with E(DMC) stably cycled for 1000 h under the same testing condition with a depth of discharge of 17.1%, which was 15 times longer than that with E(H_2O). As shown in Figure 4b, the 10 μm Zn||10 μm Zn symmetric cells with E(H_2O) failed after 43 h at the current density of 2 mA cm^{-2} and the areal capacity of 1 mAh cm^{-2}. The 10 μm Zn||10 μm Zn symmetric cells with E(DMC) stably cycled for 750 h under the same testing condition with a depth of discharge of 17.1%, which was 17 times longer than that with E(H_2O). As shown in Figure 4c, the 10 μm Zn||10 μm Zn symmetric cells with E(H_2O) failed at the 78th h at the current density of 2 mA cm^{-2} and the areal capacity of 2 mAh cm^{-2}. The 10 μm Zn||10 μm Zn symmetric cells with E(DMC) stably cycled for 600 h under the same testing condition with a depth of discharge of 34.2%, which was evidently longer than that with E(H_2O). Moreover, we evaluated the rate capability of zinc plating/stripping in both electrolytes at different current densities and areal capacities. As shown in Figure 4d, the polarization voltage of zinc plating/stripping increased with the increase of current density in both electrolytes. Comparatively, the Zn||Zn symmetric cell with E(DMC) exhibited higher polarization voltage than that with E(H_2O). To investigate the morphology and composition evolution of the metallic zinc, we characterized the Zn||Zn symmetric cells after pre-cycling (Figure S9, Supporting Information). Optical images showed that a thicker deposition was formed on the surface of the metallic zinc pre-cycled in E(H_2O), while the deposition layer of the metallic zinc pre-cycled in E(DMC) was thinner (Figure S10, Supporting Information). Likewise, SEM images showed that massive bulky depositions could be observed on the surface of the metallic zinc after pre-cycling in E(H_2O) (Figure S11, Supporting Information). In comparison, the morphology of the metallic zinc after pre-cycling in E(DMC) was comparatively denser and more even (Figure S12, Supporting Information). To evaluate the electrochemical reversibility of zinc plating/stripping, we evaluated the Coulombic efficiency of the Zn||Ti half-cells. As shown in Figure 4e, the 10 μm Zn||20 μm Ti half-cell with E(H_2O) overcharged at the 11th cycle. While the 10 μm Zn||20 μm Ti half-cell stably ran for 75 cycles, whose average Coulombic efficiency was 99.3% in the last 25 cycles. As shown in Figure 4f, the 1st Coulombic efficiency of the 10 μm Zn||20 μm Ti half-cell with E(H_2O) was 50.82%, whose polarization voltage was 119 mV. The 1st Coulombic efficiency of the 10 μm Zn||20 μm Ti half-cell with E(DMC) was 80.46%, whose polarization voltage was 205 mV. It suggests that the adoption of E(DMC) can effectively improve the electrochemical stability and reversibility of metallic zinc. The above results demonstrated the improvements of E(DMC) on the electrochemical stability and reversibility of zinc plating/stripping.

To evaluate the electrochemical performance of the metallic zinc electrode in full cells, we fabricated the Zn||PANI full cells. As shown in **Figure** 5a, the cyclic voltammetry curves of the Zn||PANI full cells with both electrolytes exhibited generally identical patterns. It suggests that the adoption of E(DMC)

remained the same redox behavior in the PANI cathodes with E(H_2O). To further evaluate the electrochemical performance of the Zn||PANI full cells at different current densities, we performed the rate capability tests. As shown in Figure 5b, the discharge capacity of the Zn||PANI full-cell with E(H_2O) at the low current density was lower than that with E(DMC), which was ascribed to the regulatory effect of the electrochemical side reactions in E(DMC). With the increase of the current densities, the discharge capacity of the Zn||PANI full-cell with E(DMC) gradually became lower than that with E(H_2O), which was attributed to its inferior mass transfer. As shown in Figure 5c, with the increase of the current density, the discharge capacity of the 10 µm Zn||≈8.0 mg cm^{-2} PANI full-cell with E(H_2O) gradually became higher than that with E(DMC), which resulted from the inferior kinetic performance in E(DMC). To fully evaluate the electrochemical performance of Zn||PANI full cells with both electrolytes, we performed the galvanostatic cycling test at the current density of 0.2 A g^{-1} in a high mass loading condition. As shown in Figure 5d, the 10 µm Zn||9.5 mg cm^{-2} PANI full-cell with E(H_2O) failed at the 50th cycle, whose capacity retention was 74.4%. The 10 µm Zn||9.3 mg cm^{-2} PANI full-cell with E(DMC) stably ran for 129 cycles, whose capacity retention was 87.6%. As shown in Figure 5e, the 1st discharge capacity of the Zn||PANI full-cell with E(H_2O) was 0.64 mAh cm^{-2}, and that with E(DMC) was 0.67 mAh cm^{-2}, which was slightly improved. In comparison, the discharge capacity of the Zn||PANI full-cell with the aprotic electrolyte was evidently lower than that with the protic electrolyte due to the lack of hydrogen ions (Figure S13, Supporting Information). However, although the water content in E(DMC) was significantly lower than that in E(H_2O), the discharge capacity of the Zn||PANI full-cell remained the same. It confirms that the adoption of E(DMC) maintains the intrinsic advantages of E(H_2O) while effectively regulating the activity of water molecules. Based on its lean-water and controllable solvation environment, E(DMC) exhibited more balanced and comprehensive characteristics in the complex structure-performance relationship, which provides important insights for the practical application of aqueous zinc metal batteries.

3. Conclusion

In summary, we demonstrated an ultra-thin and high areal capacity metallic zinc anode by utilizing crystalline water with a stable stoichiometric ratio. Different from conventional electrolytes, the designed electrolyte can form a stable and controllable solvation environment by directly utilizing the crystalline water from commercial zinc salts. It can effectively suppress the reactivity of water molecules and diminish the detrimental corrosion on the metallic zinc anode, while preserving the inherent advantages of water molecules, including great kinetic performance in electrolytes and the H^+ capacity contribution in cathodes. Based on the comprehensive performance of the designed electrolyte, the 10 µm Zn||10 µm Zn symmetric cell stably cycled for 1000 h at the current density of 1 mA cm^{-2} and the areal capacity of 1 mAh cm^{-2}, whose depth-of-discharge is over 17.1%. The 10 µm Zn||20 µm Ti half-cell exhibited the average Coulombic efficiency of 99.3% within 75 cycles. Zn||PANI full-cells with high mass loading achieve great electrochemical performance. This research presents a valuable approach to balancing the overall activity of water molecules in aqueous zinc metal batteries.

Supporting Information

Supporting Information is available from the Wiley Online Library or from the author.

Acknowledgements

The authors thank the National Natural Science Foundation of China (52061160482 and 52273297), the Key R&D Plan of the Ministry of Science and Technology (2022YFB2404501), the Guangdong Provincial Key Laboratory of Thermal Management Engineering & Materials (2020B1212060015), the Shenzhen Technical Project (GJHZ20210705143000002 and KCXST20221021111401003), the Shenzhen Outstanding Talents Training Fund, and the Shenzhen Geim Graphene Center for financial supports.

Conflict of Interest

The authors declare no conflict of interest.

Data Availability Statement

The data that support the findings of this study are available in the supplementary material of this article.

Keywords

aqueous electrolyte, crystalline water, dimethyl carbonate, zinc metal battery, zinc perchlorate hexahydrate

Received: June 13, 2024
Revised: June 28, 2024
Published online: July 10, 2024

[1] a) Y. Zhu, G. Liang, X. Cui, X. Liu, H. Zhong, C. Zhi, Y. Yang, *Energy Environ. Sci.* **2024**, *17*, 369; b) S. W. D. Gourley, R. Brown, B. D. Adams, D. Higgins, *Joule* **2023**, *7*, 1415; c) H. P. Li, R. Z. Zhao, W. H. Zhou, L. P. Wang, W. Li, D. Y. Zhao, D. L. Chao, *JACS Au* **2023**, *3*, 2107.
[2] a) L. Qian, R. Yao, C. Yang, *ChemElectroChem* **2023**, *10*, 202300287; b) Q. Li, A. Chen, D. H. Wang, Z. X. Pe, C. Y. Zhi, *Joule* **2022**, *6*, 273; c) J. Hao, X. Li, X. Zeng, D. Li, J. Mao, Z. Guo, *Energy Environ. Sci.* **2020**, *13*, 3917; d) L. Ma, M. A. Schroeder, O. Borodin, T. P. Pollard, M. S. Ding, C. Wang, K. Xu, *Nat. Energy* **2020**, *5*, 743.
[3] a) D. J. Dong, T. R. Wang, Y. Sun, J. Fan, Y. C. Lu, *Nat. Sustainability* **2023**, *6*, 1474; b) S. Y. Gao, B. M. Li, H. Y. Tan, F. Xia, O. Dahunsi, W. Q. Xu, Y. Z. Liu, R. Y. Wang, Y. W. Cheng, *Adv. Mater.* **2022**, *34*, 2201510; c) F. Wang, O. Borodin, T. Gao, X. Fan, W. Sun, F. Han, A. Faraone, J. A. Dura, K. Xu, C. Wang, *Nat. Mater.* **2018**, *17*, 543; d) Q. Zhang, Y. Ma, Y. Lu, L. Li, F. Wan, K. Zhang, J. Chen, *Nat. Commun.* **2020**, *11*, 4463.
[4] L. Qian, H. Zhu, T. Qin, R. Yao, J. Zhao, F. Kang, C. Yang, *Adv. Funct. Mater.* **2023**, *33*, 2301118.
[5] a) R. Yao, L. Qian, Y. M. Sui, G. Y. Zhao, R. S. Guo, S. Y. Hu, P. Liu, H. J. Zhu, F. C. Wang, C. Y. Zhi, C. Yang, *Adv. Energy Mater.* **2022**, *12*,

2102780; b) R. Yao, L. Qian, G. Zhao, H. Zhu, T. Qin, C. Xiao, H. Lin, F. Kang, C. Zhi, C. Yang, *J. Mater. Chem. A* **2023**, *11*, 1361; c) C. Xiao, R. Yao, H. Zhu, L. Qian, C. Yang, *Chem. Commun.* **2022**, *58*, 10088; d) R. R. Zhao, H. F. Wang, H. R. Du, Y. Yang, Z. H. Gao, L. Qie, Y. H. Huang, *Nat. Commun.* **2022**, *13*, 3252.

[6] a) L. Qian, W. T. Yao, R. Yao, Y. M. Sui, H. J. Zhu, F. C. Wang, J. W. Zhao, C. Y. Zhi, C. Yang, *Adv. Funct. Mater.* **2021**, *31*, 2105736; b) F. Bu, Y. Gao, W. Zhao, Q. Cao, Y. Deng, J. Chen, J. Pu, J. Yang, Y. Wang, N. Yang, T. Meng, X. Liu, C. Guan, *Angew. Chem., Int. Ed.* **2024**, *63*, 202318496; c) K. Ouyang, S. Chen, W. Ling, M. Cui, Q. Ma, K. Zhang, P. Zhang, Y. Huang, *Angew. Chem., Int. Ed.* **2023**, *62*, 202311988; d) C. Lin, L. He, P. Xiong, H. Lin, W. Lai, X. Yang, F. Xiao, X.-L. Sun, Q. Qian, S. Liu, Q. Chen, S. Kaskel, L. Zeng, *ACS Nano* **2023**, *17*, 23181.

[7] a) D. Wang, D. Lv, H. Liu, S. Zhang, C. Wang, C. Wang, J. Yang, Y. Qian, *Angew. Chem., Int. Ed.* **2022**, *61*, 202212839; b) H. Fan, H. Zhang, Q. Liu, M. Li, L. Liu, J. Gao, Q. Zhang, E. Wang, *ACS Energy Lett.* **2023**, *8*, 4338; c) S. Liu, J. P. Vongsvivut, Y. Wang, R. Zhang, F. Yang, S. Zhang, K. Davey, J. Mao, Z. Guo, *Angew. Chem., Int. Ed.* **2023**, *62*, 202215600; d) P. X. Xiong, Y. B. Kang, N. Yao, X. Chen, H. Y. Mao, W. S. Jang, D. M. Halat, Z. H. Fu, M. H. Jung, H. Y. Jeong, Y. M. Kim, J. A. Reimer, Q. Zhang, H. S. Park, *ACS Energy Lett.* **2023**, *8*, 1613.

[8] a) G. Zampardi, F. La Mantia, *Nat. Commun.* **2022**, *13*, 687; b) X. Y. Yu, Z. G. Li, X. H. Wu, H. T. Zhang, Q. G. Zhao, H. F. Liang, H. Wang, D. L. Chao, F. Wang, Y. Qiao, H. S. Zhou, S. G. Sun, *Joule* **2023**, *7*, 1145; c) S. Xin, X. Zhang, L. Wang, H. J. Yu, X. Chang, Y. M. Zhao, Q. H. Meng, P. Xu, C. Z. Zhao, J. H. Chen, H. C. Lu, X. R. Kong, J. L. Wang, K. Chen, G. Huang, X. B. Zhang, Y. Su, Y. Xiao, S. L. Chou, S. L. Zhang, Z. P. Guo, A. B. Du, G. L. Cui, G. J. Yang, Q. Zhao, L. B. Dong, D. Zhou, F. Y. Kang, H. Hong, C. Y. Zhi, et al., *Sci. China Chem.* **2024**, *67*, 13; d) X. Zhang, L. Zhang, X. Jia, W. Song, Y. Liu, *Nano-Micro Lett.* **2024**, *16*, 75.

[9] R. Yao, Y. X. Zhao, L. M. Wang, C. X. Xiao, F. Y. Kang, C. Y. Zhi, C. Yang, *Energy Environ. Sci.* **2024**, *17*, 3112.

[10] a) Y. Lv, Y. Xiao, L. Ma, C. Zhi, S. Chen, *Adv. Mater.* **2022**, *34*, 2106409; b) Y. S. Meng, V. Srinivasan, K. Xu, *Science* **2022**, *378*, 3750; c) Y. Liang, Y. Yao, *Nat. Rev. Mater.* **2022**, *8*, 109; d) Z. Khan, D. Kumar, X. Crispin, *Adv. Mater.* **2023**, *35*, 2300369.

[11] a) C. Wang, P. Chen, Y. Li, G. Zhao, Y. Liu, Y. Lu, *J. Catal.* **2016**, *344*, 173; b) S. Beebi, S. M. Nayeem, C. Rambabu, *J. Therm. Anal. Calorim.* **2019**, *135*, 3387.

[12] a) X. Fan, L. Chen, X. Ji, T. Deng, S. Hou, J. Chen, J. Zheng, F. Wang, J. Jiang, K. Xu, C. Wang, *Chem* **2018**, *4*, 174; b) M. B. Patel, A. Agarwal, H. D. Bist, *J. Raman Spectrosc.* **1983**, *14*, 406; c) W. W. Rudolph, C. C. Pye, *J. Solution Chem.* **1999**, *28*, 1045.